BBA - Bioenergetics 1860 (2019) 286–296

Contents lists available at ScienceDirect

BBA - Bioenergetics

journal homepage: www.elsevier.com/locate/bbabio

Mapping the excitation energy migration pathways in phycobilisomes from the cyanobacterium *Acaryochloris marina*

Dariusz M. Niedzwiedzki[a,b,c,*], Shira Bar-Zvi[d], Robert E. Blankenship[c,e,f], Noam Adir[d]

[a] Department of Energy, Environmental & Chemical Engineering, Washington University in St. Louis, St. Louis, MO 63130, USA
[b] Center for Solar Energy and Energy Storage, Washington University in St. Louis, St. Louis, MO 63130, USA
[c] Photosynthetic Antenna Research Center, Washington University in St. Louis, St. Louis, MO 63130, USA
[d] Schulich Faculty of Chemistry, Technion-Israel Institute of Technology, Haifa 32000, Israel
[e] Department of Biology, Washington University in St. Louis, St. Louis, MO 63130, USA
[f] Departments of Chemistry, Washington University in St. Louis, St. Louis, MO 63130, USA

A B S T R A C T

In this study, we use ultrafast time-resolved absorption and fluorescence spectroscopies to examine *A. marina* phycobilisomes isolated from cells grown under light of different intensities and spectral regimes. Investigations were performed at room temperature and at 77 K. The study demonstrates that if complexes are stabilized by high phosphate (900 mM) buffer, there are no differences between them in temporal and spectral properties of fluorescence. However, when the complexes are allowed to disassemble into trimers in low phosphate (50 mM) buffer, differences are clearly observed. The fluorescence properties of intact or disassembled phycobilisomes from cells grown in low intensity white light are unresponsive to variation in phosphate concentration. This antenna complex was further studied in detail with application of femtosecond time-resolved absorption at room temperature. Combined spectroscopic and kinetic analysis of time-resolved fluorescence and absorption data of this antenna allowed us to identify spectrally different forms of phycocyanobilins and to propose a simplified model of how they could be distributed within the phycobilisome structure.

1. Introduction

Cyanobacteria are prokaryotic autotrophic organisms that perform oxygenic photosynthesis in a wide variety of ecological niches. With only limited mobility [1], these organisms must cope with both normal variation in light intensity and wavelength distribution as well as preventing damage from occurring at very high light intensities [2–4], or deleterious combinations of light and other environmental factors (such as temperature) [5]. Different species have developed different mechanisms to achieve simultaneous photosynthetic efficiency and survival. These mechanisms have evolved to affect either the light-harvesting antenna complexes (LHC), the reaction centers or both [2,3]. Mechanisms that affect LHC include complementary chromatic acclimation [6,7], complex assembly alterations [8], orange carotenoid protein dependent non-photochemical quenching [9], etc. Modifications of LHC can alter excitation energy transfer (EET) pathways, leading to improved efficiency (at low light intensities or at non-optimal wavelengths) or limitation of EET (at high light intensities) to prevent damage or improve the total efficiency with respect to a specific environmental condition. Understanding the changes that occur in LHC EET pathways at the molecular level is difficult at higher levels of complexity (in vivo or with isolated intact complexes) due to the overlap of a very large number (> 1000) of similar pigments [10]. However, it is only by studying these systems in their higher levels of complexity that a truly better understanding of the entire photosynthetic process can be achieved.

The cyanobacterium *Acaryochloris* (*A.*) *marina* was first described in 1996, after being isolated from a colonial ascidian, *Lissoclinum patella* [11]. Further study, on cultured cells, showed the presence of a unique phycobilisome (PBS), composed of single rods of a length and width that was interpreted as containing eight phycobiliprotein (PBP) trimers [12–14]. All trimers contain three monomers, with each monomer assembled from two homologous subunits called α and β [15,16]. The rods were not found to be associated with all of the thylakoid membranes (as is typically the case for PBS in other organisms); rather they were found to be assembled in semi-crystalline arrays in only a few regions of the membranes [17]. Analysis of isolated rods indicated that six trimers are assembled into three hexamers, proposed to contain only the phycocyanin (PC) PBP, while a terminal hexamer is assembled from a PC trimer associated with a trimer composed of the allophycocyanin (APC) PBP [12,13]. More structural information on various types of PBS can be found in recent reviews on PBS architectures and functions

* Corresponding author at: Department of Energy, Environmental & Chemical Engineering and Center for Solar Energy and Energy Storage, Washington University in St. Louis, St. Louis, MO 63130, Campus Box 1180, USA.
E-mail address: niedzwiedzki@wustl.edu (D.M. Niedzwiedzki).

https://doi.org/10.1016/j.bbabio.2019.01.002
Received 16 August 2018; Received in revised form 17 December 2018; Accepted 25 January 2019
Available online 28 January 2019
0005-2728/

[18,19].

The growth conditions reported in early reports are variable, with light intensities between 10 and 100 μE $m^{-2} s^{-1}$ [12,13], with one report that compared cells grown in low white (5 μE $m^{-2} s^{-1}$), high white (100 μE $m^{-2} s^{-1}$) red or green light [20]. In most reports, growth was performed with continuous illumination while a minority used night/day illumination regime [21]. It has been shown that the amount of PBS to Chl *d* increases in low white light growth [20].

We have recently described the functional analysis of *A. marina* PBS (AmPBS) [22] and PC (AmPC), isolated from cells grown in low white light (24 h illumination, 3–10 μE $m^{-2} s^{-1}$) [16]. The AmPBS exhibited red-shifted emission (673 nm) although shown to lack APC by mass spectrometry [16,22]. Since APC is usually the component of the PBS that is considered to have the most red-shifted emission, this observation came as a surprise. In addition, transfer of the isolated intact AmPBS from buffer with high concentrations of phosphate (hPBu) to low concentration (lPBu) (known to induce disintegration of the PBS to its component trimers and prevent inter-trimer EET) revealed that these AmPC trimers also exhibit a substantial red-shifted fluorescence emission, peaking at 660 nm at 77 K. X-ray crystallographic and MS analysis of the AmPC from these low white-light-grown cells revealed that trimers are heterogeneous, containing the gene products of both α-subunit isoforms and a smaller heterogeneity in the β-subunits. We have proposed that it is the presence of multiple gene products that affords the strong red shift in the emission of AmPC (and APC-less AmPBS) [16]. In this work, we present a follow up study on the whole *A. marina* phycobilisomes (AmPBS) isolated from cells grown under light of different intensities and spectral regimes with application of various static and time-resolved optical spectroscopies at room temperature (RT) and at 77 K. We performed comparative fluorescence study of the set of AmPBS complexes resuspended in high (900 mM) and low (50 mM) phosphate buffers to find any potential differences between them. Subsequently, the representative AmPBS that showed the smallest response to the destabilizing effect of low concentration of phosphate was further investigated in detail with application of time-resolved absorption at RT in high phosphate buffer to assure sample integrity. Combined spectroscopic and kinetic analysis of time-resolved fluorescence and absorption data of this antenna form allowed us to identify spectrally different forms of phycocyanobilins (PCB) and propose a simplified model of how they may be distributed within this specific AmPBS complex.

2. Materials and methods

2.1. A. marina cyanobacterial growth

A. marina strain MBIC11017 cells were grown in a 2 L growth chamber with MBG11 medium supplemented with 5% CO_2 in air at RT, with fluorescent lamp illumination. Cells were grown for 7 to 14 days in constant white LED light (low white (lWL): 3.5–10 μE $m^{-2} s^{-1}$, high white (hWL): 10–80 μE $m^{-2} s^{-1}$, green light (GL): 450–550 nm, red light (RL): > 600 nm), collected by centrifugation, and frozen at −20 °C.

2.2. Isolation of AmPBS

3–6 g of frozen cells were thawed and re-suspended in high ionic strength isolation buffer (900 mM phosphate buffer, pH 7.0 was used for all procedure steps), and disrupted by a microfluidizer (30 psi). Following a 10 min centrifugation at 10,000 rpm to pellet the unbroken cells, the green-blue crude PBP solution was incubated for 1 h with 2% Triton X-100 (w/v) to remove the AmPBS from the thylakoid membranes, followed by clarification with centrifugation. The supernatant was placed on a linear sucrose gradient (0.25–1.00 M sucrose buffers) and centrifuged at 55,000 rpm (278,000 × *g*) overnight, resulting in a single band at 0.75 M sucrose.

2.3. Steady-state and time-resolved spectroscopies

Steady-state absorption spectra were recorded using a UV-1800 spectrophotometer from Shimadzu. Time-resolved fluorescence (TRF) imaging was performed using a universal streak camera system from Hamamatsu (Hamamatsu Corporation, Japan) based on the N51716-04 streak tube and the A6365-01 Bruker spectrograph (Bruker Corporation, USA) coupled to an ultrafast laser system (Spectra-Physics, USA) described in detail previously [23]. The repetition rate of the excitation laser was set to 4 MHz, corresponding to ~250 ns between subsequent pulses. The excitation beam was depolarized, focused on the sample in a circular spot of ~1 mm diameter and set to a wavelength of 540 nm and very low photon flux of ~10^{10} photons/cm^2 per pulse. Fluorescence emission was measured at a right angle to the excitation beam with a long-pass 610 nm filter placed at the entrance slit of the spectrograph. The integrity of the samples was examined by observing the photon counts in real-time over the time course of the experiment. These were constant, indicating the absence of sample photodegradation. The cryogenic measurements were carried out at 77 K, using a VNF-100 liquid nitrogen cryostat (Janis, USA). The sample was placed in 1 cm poly(methyl methacrylate) (PMMA) cuvette in plain buffers and slowly frozen. Absorbance of the sample was adjusted to 0.1 at the maximum of the absorption band. Transient absorption (TA) experiments were carried out at RT using Helios, a femtosecond time-resolved and pump-probe absorption spectrometer (UltrafastSystems, USA) coupled to a Spectra-Physics femtosecond laser system described in detail previously [24]. The energy of the excitation beam (570 nm) was set to 40 nJ, corresponding to a photon flux of 1–2 × 10^{13} photons/cm^2 per pulse (the beam was focused to ~1 mm dimeter spot on the sample, laser repetition was set to 1 kHz). The sample was placed in a 2 mm quartz cuvette and adjusted to an absorbance of ~0.3–0.5 at the maximum of the absorption band. In order to avoid photobleaching during measurements, the sample was vigorously stirred with a magnetic stirrer.

2.4. Data processing and analysis

Prior to further analysis all TRF datasets were subjected to singular value decomposition (SVD), a least square estimator of the original data leading to significant noise reduction [25]. Temporal chirp in the TA datasets was corrected using Surface Xplorer software (UltrafastSystems, USA) by building a dispersion correction curve from a set of initial times of transient signals obtained from single wavelength fits of representative kinetics. Both TRF and TA datasets were first globally fitted with application of a simple fitting model that assumes an irreversible direction of excitation decay from fastest to slowest decaying states. According to this model, the transient signal at any time delay and wavelength, ΔA(*t*,λ) or Fl(*t*,λ), can be decomposed to a superposition of *n*th $C_i^S(t) \cdot EAS_i(\lambda)$ products [26]:

$$\Delta A,\ Fl(t,\lambda) = \sum_{i=1}^{n} C_i^S(t) EAS_i(\lambda) \quad (1)$$

where C_i (*t*) is time-dependent concentration of *i*th EAS (evolution associated spectrum) defined by a kinetic model of sequential decay:

$$\frac{dC_i^S(t)}{dt} = k_{i-1}C_{i-1}^S(t) - k_i C_i^S(t),\ i \neq 1,\ k_{i-1} > k_i \quad (2)$$

and the first EAS concentration, $C_1(t)$, is populated by the excitation pulse represented by the instrument response function (IRF) of the spectrometer:

$$\frac{dC_1^S(t)}{dt} = IRF(t) - k_1 C_1^S(t) \quad (3)$$

Global analysis was done using CarpetView software (Light Conversion, Lithuania). The IRF was mimicked by a Gaussian with the

full width at half maximum (FWHM) of ~200 fs for TA datasets and 0.35 ns for TRF datasets. In order to distinguish global fitting results of TRF and TA datasets, EAS components are specified as EADS and EAFS – evolution associated difference/fluorescence spectra. Target analysis of transient absorption datasets was also performed. According to this kind of modeling, transient absorption decay signals at any time delay and wavelength, ΔA(t, λ), can be decomposed to a superposition of *n*th $C_i^S(t) \cdot SADS_i(\lambda)$ (Species Associated Difference Spectra) products.

$$\Delta A(t,\lambda) = \sum_{i=1}^{n} C_i^S(t) SADS_i(\lambda) \quad (4)$$

where $C_i^S(t)$ are time-dependent SADS concentration defined by a kinetic model mimicking the true excitation decay pathway. While global analysis with sequential decay gives only apparent (observed) model independent decay rates, target analysis includes hidden microscopic rates [26].

3. Results and discussion

3.1. Time-resolved fluorescence at 77 K

The TRF results of AmPBSs isolated from cells grown under different light conditions (lWL, hWL, GL, RL), taken at 77 K in two different concentrations of phosphate ions (hPBu – 900 mM or lPBu – 50 mM) in the buffer are given in Fig. 1. The figure panels also contain time-integrated spectra that correspond to the expected steady-state fluorescence spectrum of each complex. The pseudo-color profiles represent fluorescence intensity (black - zero, red - maximum) recorded at various delay times after excitation.

In hPBu, all AmPBSs show very similar TRF profiles with the fluorescence maximum centered at 673 nm. However, upon disassembly in lPBu, changes between the samples start to appear. The least affected is the AmPBS from cells grown in lWL. The maximum of the fluorescence profile is still close to 673 nm. On the other hand, the most affected are the AmPBSs from cells grown under hWL and GL, with the fluorescence maximum shifted to 658 nm. Moreover, the fluorescence spectrum of the hWL AmPBS has an apparently broader spectral envelope. The fluorescence maximum of the AmPBS from cells grown in RL falls in the middle of the range between those two extremes. Shift of the fluorescence peak toward shorter wavelengths is associated with the destabilizing effect of low ionic buffer that weakens inter- trimer/hexamer interaction and excitation energy transfer. Fluorescence decay profiles were subject to global analysis (fitting) with application of a sequential model (see Materials and methods). The model assumes that excitation irreversibly jumps between different molecular species of phycocyanobilins (PCB) presumably via the route that is most efficient from an energetic point of view (toward lower energies). In global analysis, unlike in a single wavelength fitting, the fitting simultaneously interpolates all recoded decays (whole TRF profile). EAFS, the spectro-temporal components resulting from the fitting are given in Fig. 2. For better comparability, all EAFS are normalized to unity at their maxima. If the fluorescence decay lifetime of a certain EAFS was shorter than the temporal resolution of the streak camera setup (~350 ps in the time domain used in these experiments), its lifetime is noted as < IRF. The maxima of all EAFS profiles are also marked in the graphs. Satisfactory fitting required two spectro-kinetic components in all cases. In every sample, the lifetime of the shorter component is limited by the temporal resolution of the detecting system. The presence of a substantially shorter spectro-kinetic component with fluorescence maximum shifted to shorter wavelengths by 6–14 nm suggests that it is associated with emission from a spectral form of PCB that transfers excitation energy to the terminal emitter of the AmPBS immediately after excitation.

Alternatively, the fast decaying component could be associated with energetic equilibration of the emitter. However, the true amplitude of the first component is much smaller with respect to the long-lived EAFS

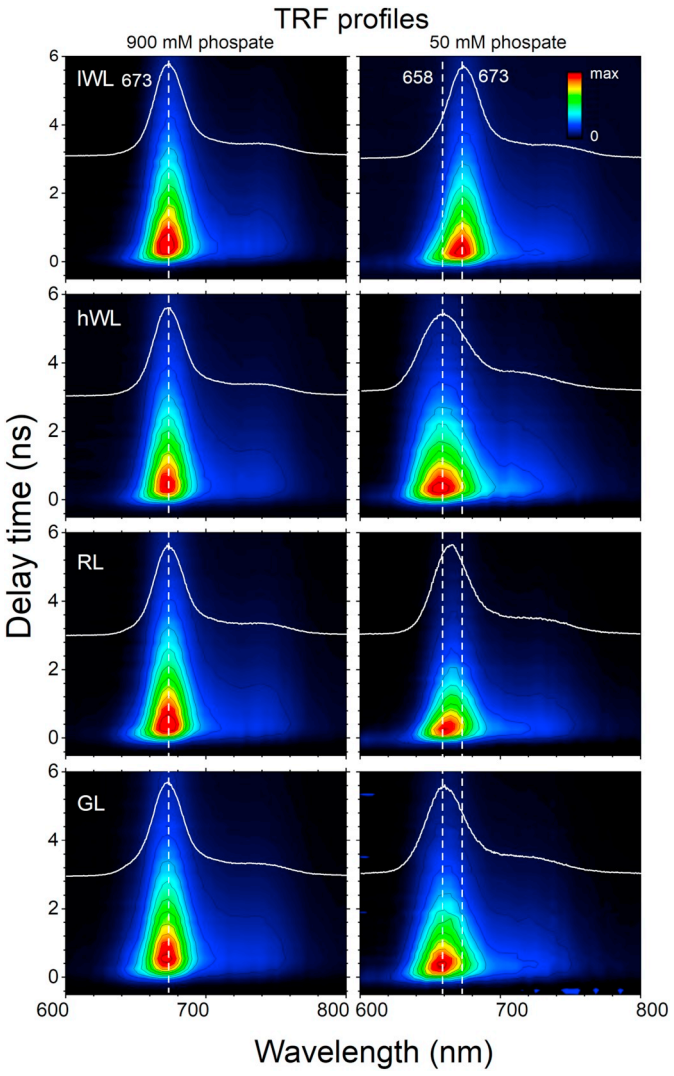

Fig. 1. Time-resolved fluorescence of the AmPBSs from cells grown in various light conditions (low white light- lWL, high white light - hWL, red light – RL and green light - GL) taken at 77 K in the buffer with high and low phosphate concentrations. The samples were excited at 540 nm. White dashed lines mark fluorescence maxima. The solid white spectra correspond to time-integrated spectra that represent the steady-state fluorescence emission.

(Fig. 2 shows both normalized for better comparability), thus it has a substantially smaller fluorescence yield and it is only possible if it is quenched (via EET) by the terminal emitter. If this EAFS component represents fluorescence from non-equilibrated terminal emitter, real amplitudes of both components should not differ significantly and only the fluorescence maximum will red-shift as time evolves. In hPBu, all AmPBSs show comparable decay lifetimes of fluorescence from terminal emitter (2.0–2.1 ns). In addition, all 2-ns EAFS share an almost identical spectral shape with maximum at 673 nm. Some variation of the position of the maximum is noticeable for faster EAFS for which the fluorescence maximum ranges between 660 and 667 nm, therefore there must be some spectral variations in absorption of particular PCBs within AmPBS rod if growth light condition is altered. More variations in the fluorescence decay dynamics accompanied with changes in fluorescence emission spectra positions are noticeable in lPBu. Lifetime of the long-lived EAFS component varies from 1.4 ns (GL) to 2.1 ns (hWL) without any apparent pattern or trend in values. In some cases, like for the hWL AmPBS, fluorescence lifetime is not affected regardless of the fact that the fluorescence emission spectrum substantially shifts to shorter wavelengths by 15 nm and spectral broadening is noticeable.

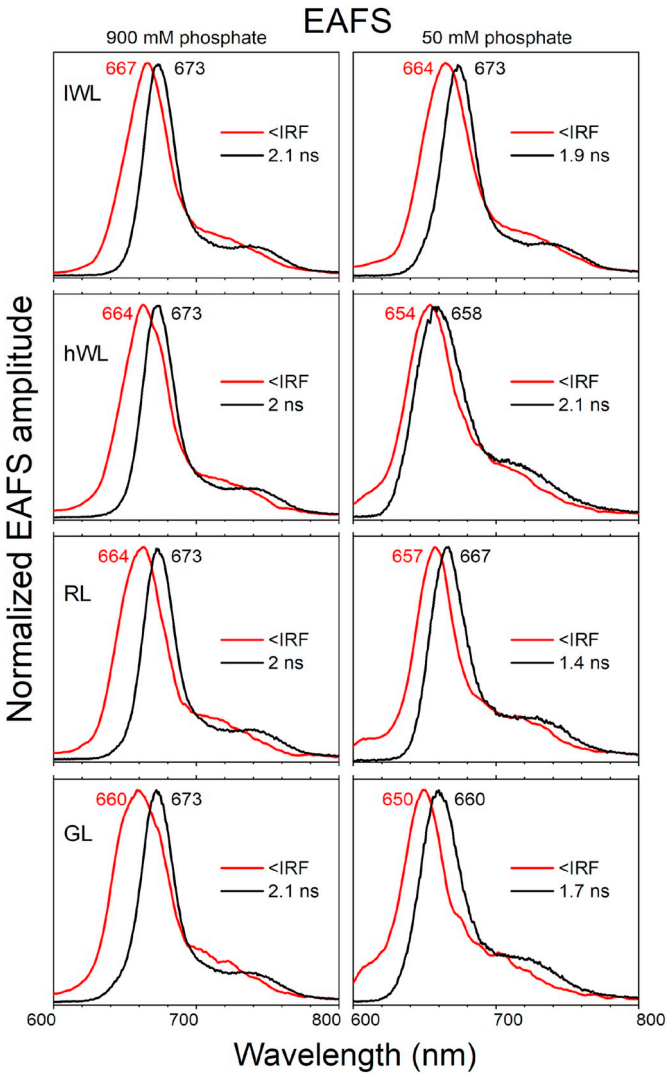

Fig. 2. Spectro-temporal components (EAFS) from global fitting analysis of 77 K TRF of the AmPBSs from cells grown in various light conditions. See Fig. 1 for definitions.

On the other hand the RL AmPBS that shows the largest change in fluorescence decay lifetime shows much smaller spectral shift of fluorescence mission spectrum toward shorter wavelengths. Therefore, there is no clear trend between shift of fluorescence spectrum and fluorescence dynamics. The only outlier that shows essentially no response (position and dynamics of fluorescence emission) to low phosphate concentration is the lWL AmPBS that according to our previous studies does not contain APC in its structure [16]. The fact that all other AmPBSs show different variability in position and fluorescence dynamics in low ionic strength buffer, shows that all of them most likely incorporate APC in some quantities and the spectral shift manifests energetic decoupling of APC from the rest of the AmPBS rod [14]. Alternatively, these forms of PBS have a smaller amount of PC-based terminal emitter than those obtained from lWL grown cells. It is quite intriguing because in order to produce the GL and RL AmPBS the bacterium culture was illuminated using the same high white light lamp only filtered by color. Therefore, the total amounts of green or red photons were equal to the amount of green/red photons experienced by bacterium producing the hWL AmPBS. From those three, the GL and hWL AmPBSs show the smallest differences suggesting that the photoreceptor that "senses" light intensity most likely absorbs green light. It may not be surprising as it is known that cyanobacteria produce various phytochromes called cyanobacteriochromes responsible, among others, for complementary chromatic acclimation, that absorb in blue-green spectral ranges [27–29].

From our perspective, from the set of four AmPBSs the most interesting is the lWL AmPBS due to the fact that functionally it performs as a typical PBS though it is built entirely on PC [16]. Therefore, further studies and analyses were exclusively concentrated on this sample resuspended in hPBu. It is quite interesting to investigate the mechanisms that might be responsible for tweaking spectral properties of particular PC units in ways that assure long-wavelength absorption/emission necessary for proper energetic coupling of this AmPBS with the PSII complex.

3.2. 77 K vs RT time-resolved fluorescence of the lWL AmPBS

A relevant question here is if outcomes from analysis of 77 K TRF can be directly used to explain results recorded at RT that are apparently more physiologically relevant. Previous studies of temperature-dependence fluorescence of the AmPBS have been done for the AmPBS that was stated to contain APC and thus cannot be directly compared here [14]. However as recently shown by us [16], the existence of a strong red-shift in the emission of AmPBS is not necessarily evidence of the presence of APC.

The RT fluorescence emission spectrum of the AmPBS consists of a quite broad spectrum (Fig. 3A), suggesting that two independently fluorescing PCBs with maxima at 646 and 667 nm partially overlap on each other. Notably, the positions of those peaks are essentially identical with peaks in the fluorescence spectrum of the proposed APC-containing AmPBS [12–14], however their amplitude ratio is not the same. A simple explanation could be that both PCBs are not perfectly energetically coupled (it could be intra-PC or inter-PC coupling). However, if it is true, cryogenic temperature should amplify the effect and the fluorescence emission spectrum would clearly split into two bands. Previously, it was shown that it is correct only for fluorescence measurements taken in lPBu in which energetic coupling in the APC-containing PBS is truly disrupted [12,13]. However, if the AmPBS is gently frozen in hPBu, the florescence peak substantially sharpens and appears as a single peak at ~670 nm [12–14], similarly as it is also observed in these studies.

Comparable fluorescence emission spectra of the lWL AmPBS at RT and 77 K, to the above-mentioned literature example are shown in Fig. 3A. The panel shows fluorescence time-integrated spectra corresponding to the expected steady-state fluorescence emission spectra. This figure better visualizes the effect of cryogenic temperature on the fluorescence emission spectral shape. The RT TRF dataset of the lWL AmPBS was also globally fitted with application of the irreversible, sequential decay of the excitation. Successful fitting required two (same as at 77 K) EAFS components. Their amplitude spectra (normalized) are given in Fig. 3B. The first EAFS, with time-resolution limited lifetime, spectrally fits very well into the position of energetically higher PCB. However, the second EAFS still carries the same spectral characteristics as the steady-state fluorescence spectrum, thus fluorescence from both spectral forms of PCB share the same apparent decay rate of $(1.7\ \text{ns})^{-1}$.

At RT, the lWL AmPBS absorption shows substantial spectral congestion of various spectral forms of PCB, therefore, for a rather broad PCB fluorescence spectrum, there is a non-zero overlap between fluorescence of the terminal emitter and absorption spectra of spatially close PCBs but energetically different from the terminal emitter. Those PCBs nominally have higher excited state energies, however, due to the long-wavelength tail of the absorption spectrum, spectral overlap between fluorescence of terminal emitter and their absorption is still possible.

Consequently, in addition to the intrinsic decay of the excited state of the terminal emitter into its ground state, energy transfer to neighboring PCBs may also occur. On the other hand, those excited PCBs will pass the excitation back toward the terminal emitter. It is apparent that some sort of equilibrium will be established in this system and

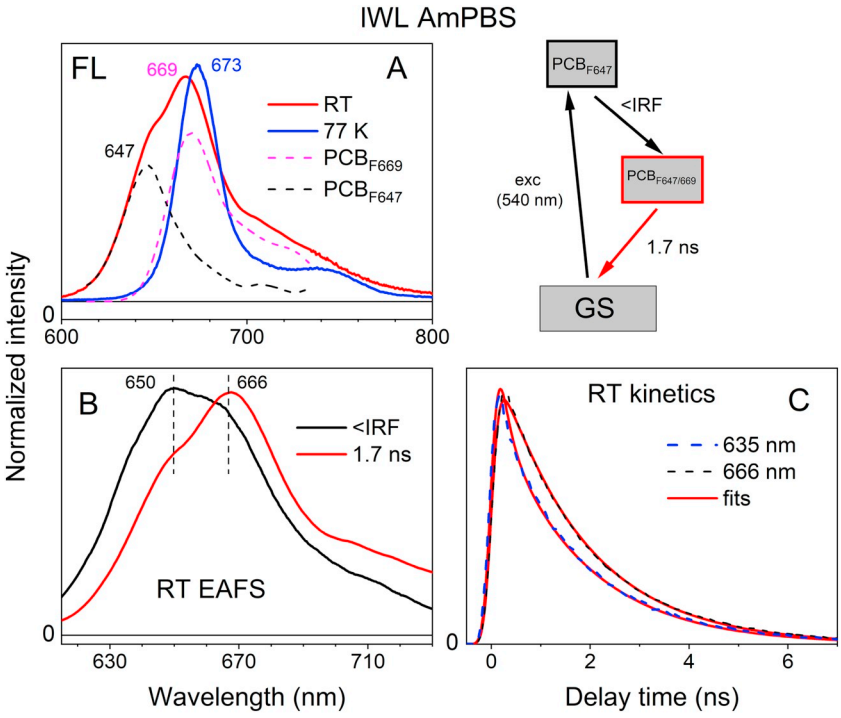

Fig. 3. Kinetic analysis of RT TRF of the lWL AmPBS; (A) RT (with hypothetical fluorescence spectra of two spectral PCB forms involved in emission) and 77 K fluorescence spectrum of the same AmPBS sample; (B) normalized EAFS components from global fitting according to the scheme given in the right top figure corner; (C) exemplary kinetic traces with fits from global analysis. EAFS – evolution associated fluorescence spectra, FL – steady state fluorescence, GS – ground state, IRF – instrument response function, PCB – phycocyanobilin.

consequently fluorescence from both spectral forms of PCB would decay with an identical apparent rate. With lowering of the temperature, as both emission and absorption spectra of PCBs sharpen and the spectral overlap required for energy transfer will be substantially reduced. As a consequence, the backward rate will be much slower, while the forward "energy funneling" rate may not be significantly affected. Consequently, the system will not reach equilibrium because the forward transfer rate would greatly overwhelm a reversed population rate and the signature of energetically higher PCB will be lost in the 77 K fluorescence spectrum of the AmPBS. Thus, the RT spectrum should simply consist of a combination of two PCB spectra, similar in shape but energetically offset. The estimates (from Gaussian decomposition) of those individual spectra are given in Fig. 3A as dashed lines. This reconstruction shows that their fluorescence maxima are 647 and 669 nm, respectively.

Because we assume that both spectral forms of PCB are in thermal equilibrium and their relative fluorescence amplitudes in the overall fluorescence spectrum of lWL AmPBS were defined, Boltzmann statistics could be applied to find the stoichiometric ratio of fluorescing PCBs as follow:

$$\frac{FA_{PCB647}}{FA_{PCB669}} = \frac{\Phi_{PCB647}}{\Phi_{PCB669}} \frac{N_{PCB647}}{N_{PCB669}} e^{\frac{E_{669}-E_{647}}{k_B T}} \quad (5)$$

where *FA* corresponds to the area of the fluorescence peak of each PCB, Φ is the fluorescence quantum yield, N_{PCB} is the number of involved PCB (state degeneracy), E – energy of the excited state of PCB (maximum of the fluorescence emission spectrum used), k_B – Boltzmann constant, $T = 293$ K. If assumed that fluorescence quantum yields of both PCBs are identical, after incorporation of remaining parameters ($\frac{FA_{PCB647}}{FA_{PCB669}} = 0.7$, $\exp\frac{E_{669}-E_{647}}{k_B T} = 0.08$) the following relation is obtained: $N_{PCB647} = 9 \times N_{PCB669}$. Therefore, if there is only one PCB$_{F669}$ pigment that plays the role of terminal emitter there are 9 PCB$_{F647}$ that are in thermal equilibrium with it at RT. However, if it is assumed that both parameters have reasonable 10% uncertainty, this number may fall anywhere between 7 and 11 range. This issue will be further elaborated in Results and discussion section.

3.3. Time-resolved absorption

Due to temporal limitation of time-resolved fluorescence measurements, the lWL AmPBS was also studied with the application of femtosecond-time resolved absorption (TA). The requirement of sample transparency limited the TA measurements only to RT as for cryogenic temperature buffer will require at least 60% (v/v) glycerol, which is known to be completely destructive for the integrity of inter-pigment energetic coupling in PBSs [30]. The studies performed on the PBS from *Synechocystis* sp. PCC 6803 demonstrated that in order to keep the PBS rod intact no > 20% glycerol should be used in experiments, however, this concentration does not produce sample transparency. It demonstrates that time–resolved and static spectroscopic studies of excitation energy migration within PBS that are done at cryogenic temperature on samples with high glycerol content may not represent what actually occurs in a native form of PBS rod and the outcome from such studies should be analyzed with caution.

Transient absorption results of the lWL AmPBS taken at RT in high ionic strength buffer (in order to maintain structural consistency) upon excitation at 570 nm are given in Fig. 4. Panel A shows pseudo-color TA profile plotted on a logarithmic time scale for better clarity. The blue regions typically correspond to negative signals associated with bleaching of the ground state absorption of various components of the AmPBS complex. The positive (red bands) are typically associated with excited state absorption. The exemplary TA spectra are shown in panel B. The results show there is an immediate onset of bleaching with minimum at ~625 nm at 60 fs after excitation that gradually shifts to longer wavelengths when time evolves. Simultaneously, two positive bands are also present, a weaker band in the 450–550 nm range and a stronger band between 650 and 720 nm. The 450–540 nm transient band gradually decays with dynamics similar to the recovery of the bleaching band, however, the transient band from the long wavelength range fades out completely after ~100 ps. In order to get more insight into excited state dynamics and their spectral characteristics, the TA data were globally analyzed with application of an excitation decay model assuming irreversible decay in sequential steps with slower rates (longer lifetimes) in subsequent steps. The results of this fitting, EADS, are shown in Fig. 5.

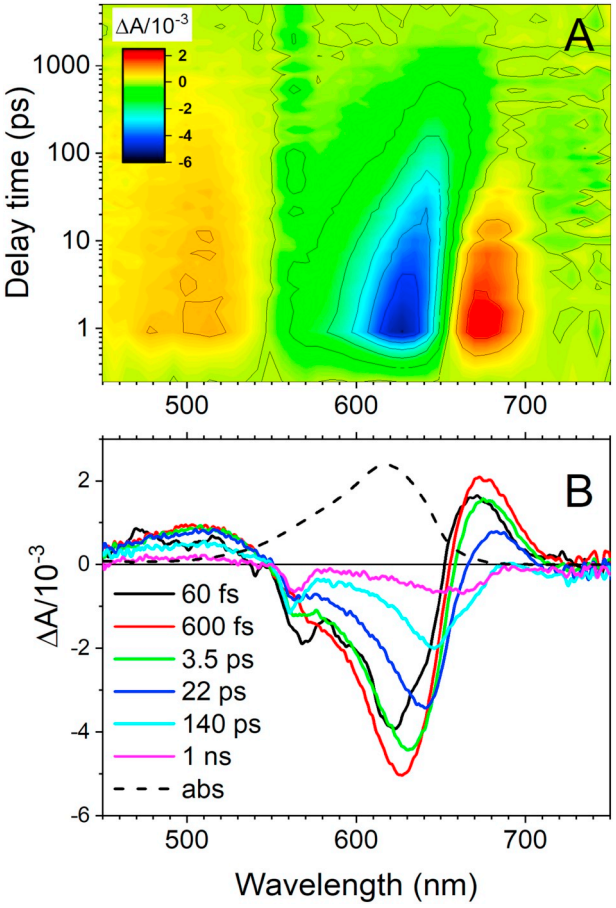

Fig. 4. Transient absorption results of the lWL AmPBS taken at RT in high ionic strength buffer. The sample was excited at 570 nm. (A) Pseudo-color TA profile, (B) Exemplary TA spectra taken at various delay times after excitation. For comparison, the scaled steady-state absorption spectrum of the lWL AmPBS (dash line) was added.

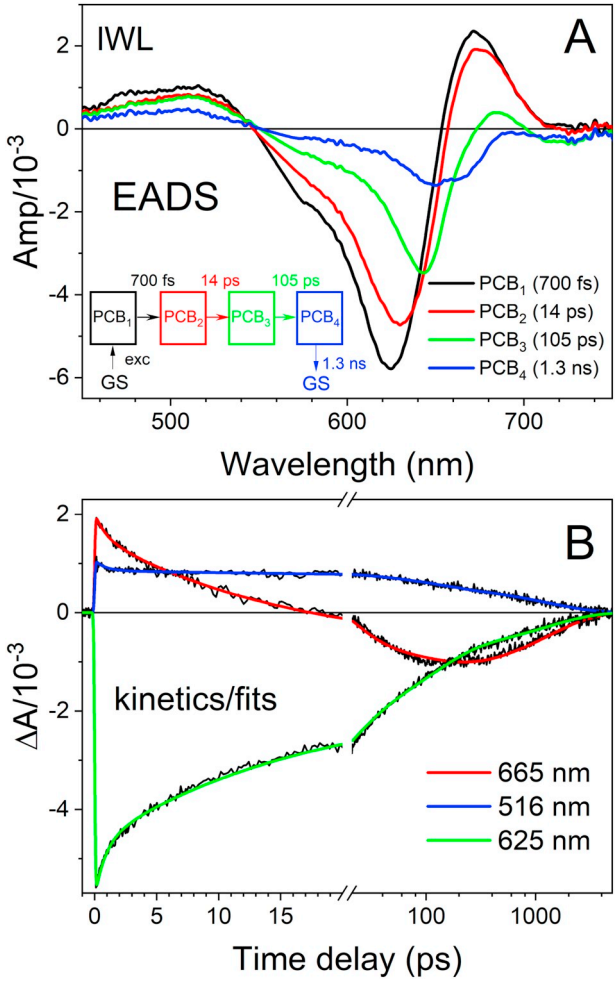

Fig. 5. Global analysis of TA datasets of the lWL AmPBS. (A) EADS with corresponding kinetic schemes used for fit; (B) exemplary kinetic traces accompanied with fits from global fitting. EADS – evolution associated decay spectra, PCB – phycocyanobilin.

It is worthwhile to compare the values obtained here with TA studies done previously on AmPBS at RT. Nganou et al. [31,32] reported kinetic components of 300 fs, 14 ps and > 200 ps. Studies performed by Theiss et al. [14] revealed the kinetic components with lifetimes of 3 ps, 14 ps and > 100 ps. In both studies kinetic analysis was performed using global fitting employing sum of exponentially decaying components (parallel decay). In this study, a different fitting model was used, however the overall results (observed lifetimes) should be independent of the choice of those models and are comparable in calculating observed lifetimes [26]. The present study shows some similarities with previous results, like the presence of a 14 ps component. However, as the AmPBS studied here may be structurally different (no APC), a complete analogy is not expected. The EADS component with a lifetime of 1.3 ns has not been reported in past studies (> 100 ps lifetime is quite ambiguous), however, it corresponds very well to the fluorescence decay lifetime of 1.7 ns observed in TRF. Those numbers are comparable but not in full agreement. The difference occurs most probably due to the fact that in TA the flux of the excitation beam is higher compared to the TRF experiment and some singlet-singlet annihilation in fluorescing pigments manifold is unavoidable (due to possible multiple excitation centers) within the rod. It will bring the observed excited state lifetime slightly lower in value.

Intuitively, a sequential fitting model should quite well mimic excitation transfer within the PBS rod as it is expected that excitation energy will be quickly funneled from “high energy” PCBs to “low energy” PCBs and finally to PCB playing role of the terminal emitter. It is very possible that irreversible sequential decay mimics excitation migration within the rod at 77 K at which thermal energy of an excited electron of the involved bilin pigment is too small to allow backward transfer to pigments with slightly higher electronic excited state energy. However, at RT the thermal energy of the excited electron of kT = ~200 cm^{-1} (T = 293 K) is close to the energetic gaps between excited state energies of PCBs in PCs in the PBS rod as seen in bleaching minima in Fig. 5A (minima are spaced between 150 and 400 cm^{-1}). Therefore, the possibility of backward transfer of excitation energy should not be ignored in each step, especially in the step between PCB_3 and PCB_4, which according to analysis of the AmPBS fluorescence, are in thermal equilibrium. Identification of the correct rates for backward transfers is not a simple task for such complex systems as the PBS. On the other hand, as RT fluorescence of the lWL PBS shows only contributions from two energetically lowest PCBs therefore $PCB_1 \rightarrow PCB_2 \rightarrow PCB_3$ steps could be assumed as irreversible, the backward transfer rates are evidently too slow and could be ignored. This is not the case for the $PCB_3 \rightarrow PCB_4$ step, if PCB_3 and PCB_4 populations are in thermal equilibrium. This is also clearly seen in EADS of TA of the lWL PBS. The spectral profile of the longest-lived EADS shows two local minima at 646 and 665 nm that would correspond to simultaneous bleaching of PCB_3 and PCB_4. Therefore, the 105 ps lifetime represents the relaxation time of PCB_3 toward equilibrium in $PCB_3 \leftrightarrow PCB_4$ pair. If it is assumed that the $PCB_3 \leftrightarrow PCB_4$ pair is a separate system, the forward and backward transfer rates (k_{34} and k_{43}) could be calculated taking under consideration that relaxation rate $(105\ ps)^{-1} = k_{34} + k_{43}$

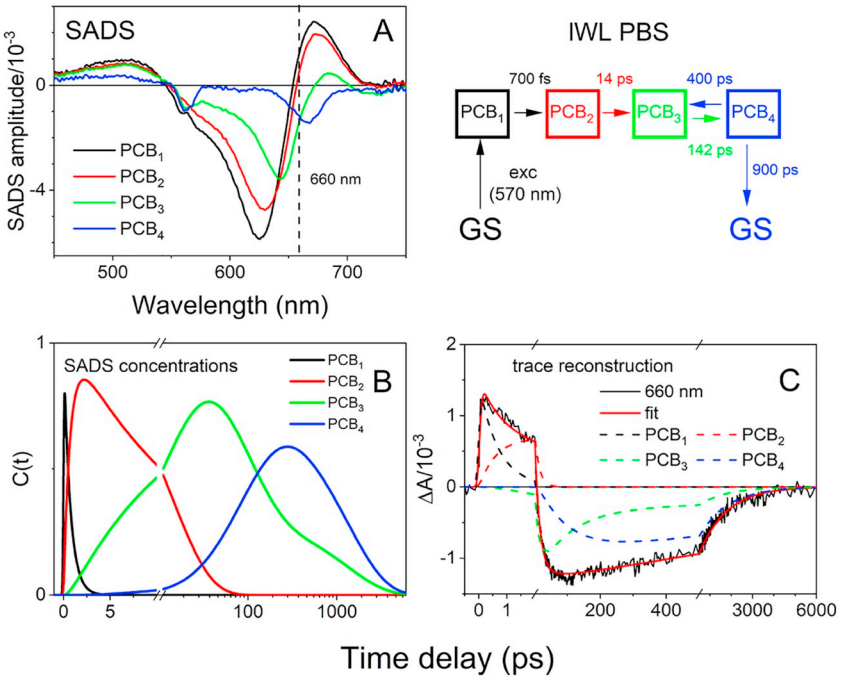

Fig. 6. Target analysis of TA datasets of the lWL AmPBS. (A) SADS with corresponding kinetic schemes used for fit, (B) SADS time-dependent concentrations demonstrating common decay rate for PB_3 and PB_4 (C) exemplary kinetic traces (660 nm) decomposed into contributions of individual molecular species; SADS – species associated difference spectra, GS – ground state, PCB – phycocyanobilin.

and equilibrium constant $K_{eq} = k_{34} / k_{43}$ that could be also calculated. However, this is a significant oversimplification, as the $PCB_3 \leftrightarrow PCB_4$ pair system is not separate. Particularly, the intrinsic decay of excited PCB_4 plays a significant role here as this decay rate can be comparable with k_{43} and cannot be simply taken out from the picture. Hence, this problem was solved numerically by modifying the sequential decay scheme of excitation from Fig. 5 by introducing forward and backward transfers between PB_3 and PCB_4 pigments and allowing these and PCB_4 intrinsic decay rates to freely float until the fit converged. The fitting results are given in Fig. 6. Due to the specificity of the model mimicking the expected pathway, this kind of fitting is typically called target analysis and spectral profiles resulting from such fitting of TA datasets are termed SADS (species associated difference spectra) [26]. Fitting results demonstrate better spectral separability of SADS - spectro-kinetic components compared to EADS, particularly the last SADS does not mix signals from ground state bleachings of the PCB_3 and PCB_4 and that is another indication that the applied fitting model of excitation deactivation pathway is more realistic than simple sequence (EADS).

It is apparent that each SADS (and to some degree EADS) is associated with a different spectral form of PCB and consists of ground state absorption bleaching (negative band), broad positive excited state absorption band with center ~500 nm and a positive sharp band in the 650–700 nm spectral range (not in all cases). The $PCB_{3,4}$ SADS show also contribution from stimulated emission (SE), appearing as negative band above 700 nm. Previously, it was argued that the 650–700 nm band also originates from excited state absorption [31]. However, such an assignment of this feature does not explain why this band fades out in the SADS profiles associated with longer-lived PCB (3 and 4), even though ESA band centered at 500 nm is still present. It is possible that this transient band has an alternative origin. It could be associated with a temporal electrochromic response of PCBs that are in the ground state and are in proximity to a PCB that is in the excited state. It should be noted that a temporary electrochromic response is not unique in light-harvesting proteins with the well-known example of LH2 from purple bacteria in which carotenoids show a strong electrochromic signal in response to excited bacteriochlorophylls [33–35]. Such an origin of this transient band fits well to its temporal characteristics as justified in the following explanation. The spectral forms of the PCBs that are initially excited (SADS PCB_1) and populated in the following EET step (SADS PCB_2) show bleaching minima (expected maximum of absorption) substantially blue-shifted and it can be assumed that those PCBs are the accessory chromophores that are present in all eight PC trimers of the lWL AmPBS. Therefore, if those are excited, a temporal change of electric field brought by a change in the molecular electric dipole will perturb the ground state energies of proximal PCB molecules, horizontally – within the same PC trimer and vertically – in the neighboring trimers, from the top and bottom. Due to different orientations of those pigments around the excited molecule, an overall effect may be similar to the electrochromic response of isotropically oriented pigments placed in an electric field. Specifically, the electrochromic response will result in an electroabsorption spectrum that is typically well approximated by the second derivative of the absorption [36]. It is apparent that this electroabsorption will also evolve as the excitation migrates to an energetically lower and smaller pool of PCBs as suggested by the decreasing amplitude of bleaching. If this hypothesis is correct, each SADS could be reconstructed from four spectral components: bleaching of the ground state absorption of the specific spectral form of the PCB, excited state absorption of the excited PCB, electroabsorption of the proximal PCBs being in the ground state and stimulated emission. An attempt to decompose each SADS into principal components is shown in Fig. 7. For simplicity, the electroabsorption spectrum was assumed to be equal to the second derivative of the absorption spectrum of the trimeric PC, energetically shifted to get the best match with the 650–700 nm band. For some SADS, the scattered laser excitation also had to be included. Stimulated emission was not included in decomposition of SADS1 and 2. There is no clear evidence it is present there, it is also possible it is mostly reabsorbed. In the ideal scenario the SADS decomposition allows us to see the true bleaching of the ground state absorption of excited PCB and by simply reversing it (sum of Gaussians in magenta), the absorption spectrum of this transient PCBs species could be obtained (solid olive line). It should be noted here that the spectral shapes are estimates. The most uncertain is the high energy (short wavelength) range of the reconstructed spectrum, as the real absorption spectrum of PCB never reaches zero in this range.

However, in the short wavelength range, the SADS are entirely dominated by ESA bands and it is uncertain how deconvolution of the SADS profile (that includes excited state absorption and bleaching of higher energy bands) should be performed. Therefore, any ground state absorption bleaching in this spectral range was not included. Regardless

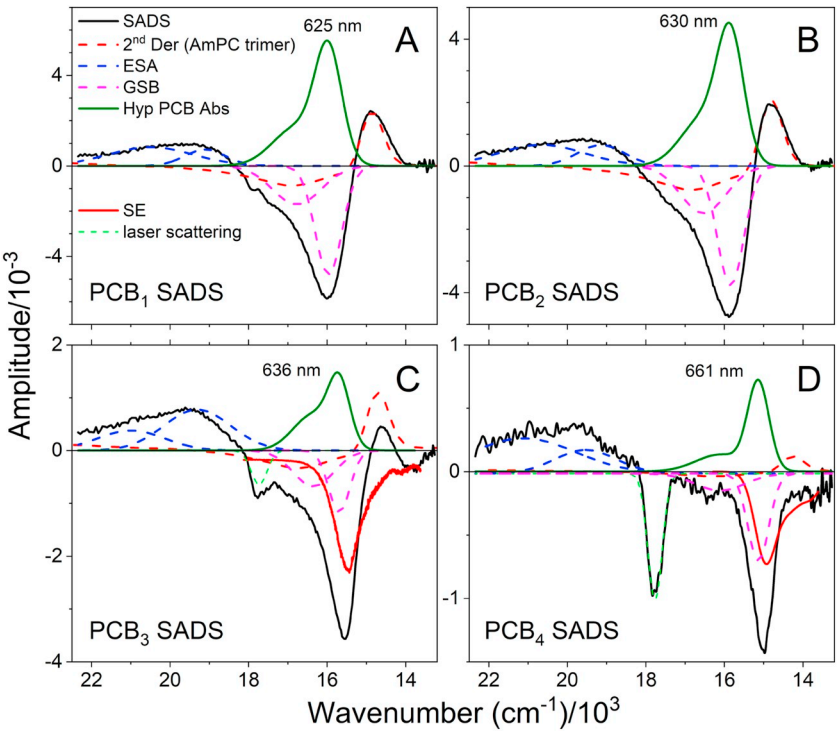

Fig. 7. Decomposition of SADS into their principal components: excited state absorption and ground state absorption bleaching of the transient PCB species and electroabsorption of neighboring PCBs in the ground state (2nd derivative of absorption of trimeric PC was used). Green dash peaks correspond to laser scattering. SE – stimulated emission, GSB – ground state bleaching, ESA – excited state absorption.

of this apparent deficiency, hypothetical ground state absorption spectra of individual PCB species (olive) are still very useful. Importantly, their maxima should correspond to true absorption maxima and their wavelengths will characterize the energetic ladder in the AmPBS rod that allows efficient funneling of excitations toward the terminal emitter. Moreover, if those spectra indeed closely imitate actual absorption spectra, at least partial reconstruction of the absorption spectrum of the whole lWL AmPBS rod is possible. The spectral reconstruction is shown in Fig. 8. For simplicity, the hypothetical absorption spectra of PCB_3 (Fig. 7C) species were used as a reference spectrum of all PCBs (but adequately energetically shifted to match their positions). Their positions were allowed to vary by < 5 nm, in order to account for possible differences between spectrometers used to record steady-state and transient absorption spectra and uncertainty of spectral deconvolution of SADS, especially SADS1 and 2. By looking at raw TA spectra it is evident that the temporal resolution of the TA spectrometer limits recording of the fastest transient PCB species expected to peak at ~600 nm or below. To complement the spectral reconstruction of the lWL AmPBS absorption, two spectral forms of equally contributing PCB were included in the procedure (as $PCB_{0(blue)/(red)}$) For better comparability of all spectral forms of PCBs, their absorption spectra were also normalized to unity and overlaid with the absorption spectrum of the lWL AmPBS on a wavelength scale (Fig. 8B).

3.4. Structural and energetic ladder of the lWL AmPBS

Each spectral form of PCB obtained from the spectral reconstruction should correspond to a specific α or β PCB type. There is consensus that PCB(β155) absorbs at short wavelength side of the PBS absorption band however, there is no consensus where specifically. Nganou [32] suggests that at RT, PCB(β155) absorption peaks at 597 nm in *A. marina* PC hexamer close to 602 nm in PC monomer from *Synechococcus* sp. PCC7002 [37]. In another study of PC from *T. vulcanus* [38] authors place maximum of the β155 PCBs absorption at ~550 nm. Gryliuk et al. [39] show that the 4 K absorption spectrum of PBS from *A. marina* partially resolves two bands at 574 nm and 599 nm. All together suggests that β155 PCB pool is somehow partitioned into two spectral forms, with absorption maxima at ~580 nm and ~600 nm, which could be spectrally resolved only at ultra-low temperatures. These positions match well to the two energetically highest PCB species at 586 and 600 nm in the spectral reconstruction in Fig. 8. The absorption maximum of PCB(α84) was suggested to peak in 622–624 nm range in PC monomers [37] and at 620 nm in PC hexamers [32]. If this tendency is maintained, it is expected to be even more blue-shifted in fully assembled PBS. This picture fits well to the PCB_1 absorption band peaking at 613 nm. Therefore, we assumed that PCB_1 corresponds to PCB(α84). The absorption bands of PCB_2 and PCB_3 are at 630 and 637 nm, respectively and correspond well to 629 and 644 nm bands resolved in the absorption spectrum of the PBS from *A. marina* recorded at 4 K [39]. We assume that those PCBs are two spectral variants of PCB(β84). Because the lWL AmPBS does not contain APC, terminally absorbing pigment at 663 nm must be also PCB, most likely PCB(β84).

Positions of absorption spectra of PCB(β84) (Fig. 8B) absorbing at 637 and 663 nm suggest that these molecular species are associated with 647 and 669 nm sub-bands in the lWL AmPBS fluorescence spectrum. It is safe to assume that all PCBs of the same family (α or β) should have comparable molar extinction coefficients, thus ratio of integrated absorption spectra (from Fig. 8A) will correspond to actual pigment stoichiometry in the PBS rod. The PCB_{A637}/PCB_{A663} ratio is ~11, confirming outcomes from thermodynamic analysis of the RT steady-state fluorescence spectrum. This information allows us to predict the hypothetical ratio of PBS species in the rod. Upon assumption that absorption spectrum is associated with idealized absorption of a single AmPBS that contains eight PC trimers the spectrum should be associated with summed contributions of 72 PCBs, 24 β155, α84 or β84, each. Simple arithmetic gives PCB molecular ratio of $β155_{blue}$:$β155_{red}$:$α84_{613}$:$β84_{630}$:$β84_{637}$:$β84_{663}$ as follow: 12:12:24:12:11:1. We assume, that the molecular extinction coefficients of various spectral variants of the same PCB type (α or β) are identical. The 12:11:1 molecular ratio for PCBs from β84 family is calculated based on ratio of the areas of their absorption bands. All this taken together allows to construct a minimal, hypothetical distribution of all molecular species (spectral variants) within the lWL AmPBS rod structure. This is shown in in Fig. 9. Fig. 9A shows structure of PC trimer from *Spirulina platensis* [40] that was schematized to show all types of PCBs. Fig. 9B shows hypothetical distribution of spectral variants of those molecular

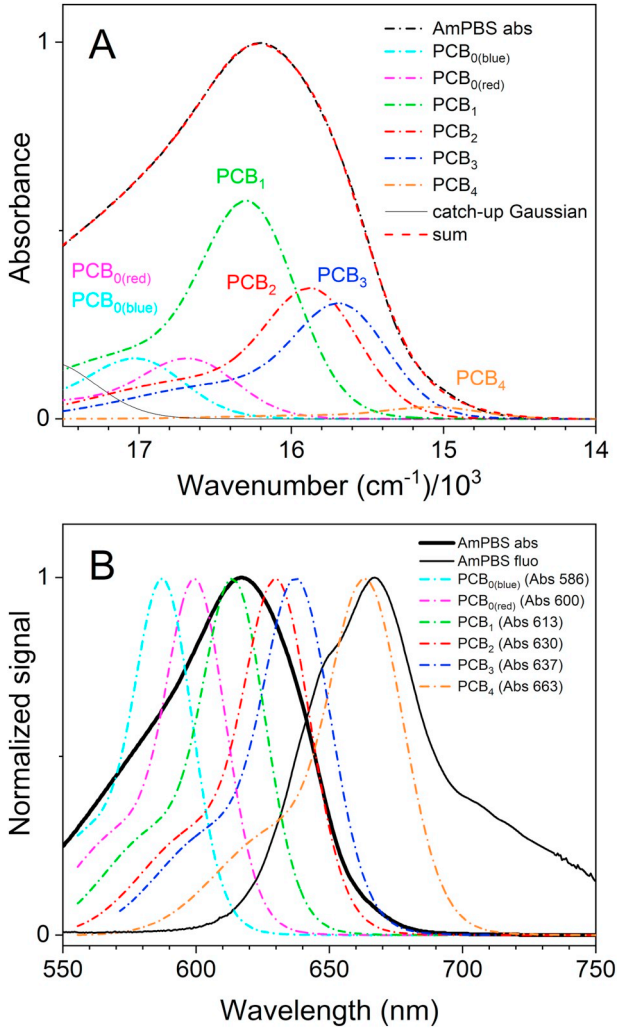

Fig. 8. Reconstruction of RT steady-state absorption spectrum of the lWL AmPBS from spectral species of PCBs detected in transient absorption. (A) Spectral reconstruction of the AmPBS absorption spectrum from the principal components. The red dash line corresponds to the sum of spectra of all principal components. The catch-up Gaussian was used to mimic any higher order vibronic bands that could not be correctly obtained from decomposition of SADS; (B) Hypothetical absorption spectra of all spectral forms of PCBs in the lWL AmPBS normalized to unity for better comparability and overlaid with RT absorption and fluorescence spectra of the lWL AmPBS.

species within AmPC trimers that form the AmPBS rod (Fig. 9C) that assures excitation energy transfer toward PSII facing interface. Note that upon complete disassembly of this AmPBS to AmPC trimers, RT fluorescence spectrum shifts to ~645 nm [16] therefore each AmPC trimer disk should contain at least one PCB($\beta84_{637}$) (according to reconstruction of steady-state fluorescence spectrum this spectral form will emit at this wavelength, see Fig. 3). The PCB($\beta84_{663}$) spectral variant is most likely associated with structural tuning, achieved only at level of whole PBS architecture and is spectrally altered upon disassembly to trimers and no longer so red-shifted. It is difficult to speculate on distribution of two spectral variants of PCB(β155) and we used a 586/600 nm "combined" symbol in all AmPC monomers. This figure includes also simplified scheme of the excitation decay pathway/migration route within arrays of PCB types and their spectral variants.

The excitation migration within the PC trimer and monomer has been extensively elaborated theoretically as well as experimentally, therefore some comparison with previous work is possible. It was demonstrated that energy transfer between nearest PCB(α_{84}) and PCB (β_{84}) chromophores in a PC trimer occurs with 0.4–1.4 ps time constant [41–45], comparable to the 700 fs observed here. On the other hand, decay of the excited PCB(β_{155}), either in monomer or trimer, was predicted and experimentally confirmed to have a lifetime of ~50 ps [46,47]. However, TA results from this study have not resolved any PCB molecular species with GSB that will match one or both spectral PCB (β_{155}) variants. It seems to be in significant disagreement however, it has to be taken under consideration that most studies of the transfer rate between bilin chromophores were limited to analysis within the horizontal plane of the PC monomer or PC trimer. Recent computational studies of the PC hexamer showed that excitation energy transfer rate between adjacent PCB(β_{155}) from PC monomers stack on each other is very fast compared to other rates and calculated at $(0.5\ ps)^{-1}$ [45]. Upon experimental conditions applied in TA study (amplified laser) it is very possible that excitation initially populates significant excess of PCB(β_{155}) that due to favorable PCB(β_{155})-PCB(β_{155}) transfer rates will annihilate and significant fraction of the signal is immediately lost within temporal resolution of the spectrometer. Therefore, because we were not able to experimentally obtain transfer rates from PCB(β_{155}) to other PCB types, on the scheme we only show most favorable routes (dashed arrows) without providing details about their dynamics.

3.5. Spectroscopic comparison of lWL AmPBS with APC containing PBS complexes

It will be also very useful to compare spectroscopic properties of the lWL AmPBS from this work with properties of other more complex, APC-containing PBSs. Very recently, a similar set of spectroscopic techniques (ps time-resolved fluorescence and fs time-resolved transient absorption) and kinetic modeling were applied to establish a functional compartmental model of the PBS from *Synechocystis* PCC 6803 (wild type, WT, and CK and CB mutants) [48,49]. For simplicity, a comparison of apparent kinetic components (observed rates) from global fitting of RT TRF or TA RT was done between lWL AmPBS and PBS from WT *Synechocystis* PCC 6803. Global fitting of TRF of WT Synechocystis PBS revealed four kinetic components with lifetimes of 15 ps, 69 ps, 139 ps and 1680 ps [49] in respect to two components with lifetimes of < 350 ps and 1.7 ns in TRF of lWL AmPBS. Shorter-lived components could not be recorded for lWL AmPBS due to temporal limitation of the instrument (350 ps here vs 24 ps in [49]). In the mentioned study, the last two kinetic components are associated with equilibration and final decay of excitations in the PBS core, within two spectral forms of APC fluorescing at ~660 and 680 nm. As seen, these dynamics are very comparable with the final equilibration and excitation decay of PC-only lWL AmPBS. Results of TA of both systems are more difficult to compare. Because different excitation intensities and excitation wavelengths (540 nm vs ~620 nm in [49]) were used in both studies analogies between a few initial kinetic components may not be apparent, although those are expected to be similar as are attributed with intra-PC rod excitation equilibration. The dynamics of the two longest-lived components are essentially the same in both PBS systems (132 ps, 1.2 ns in WT *Synechocystis* PBS vs 100 ps and 1.3 ns in lWL PBS from *A. marina*), essentially confirming what was speculated based on fitting results of TRF. Both systems show even the same final lifetime alteration from 1.7 ns (TRF) to ~1.2–1.3 ns in TA, demonstrating that both APC core and PC rod experience similar annihilation if exposed to excitation of amplified, though substantially attenuated, laser beam. In conclusion, it could be said that this and previous studies show that though both PBS are substantially structurally different (four PC hexamers assembled to a single rod in lWL *A. marina* compared to APC-containing multi-cylinder core with set of outwardly sticking rods built of three PC hexamers in *Synechocystis*), dynamics of excitation migration and relaxation bear significant resemblances. Moreover, the similarities could be so substantial that it could be difficult to distinguish PBS from each other looking only at trends in excitation dynamics without simultaneously recording their spectral signatures like maxima in TRF spectra, etc.

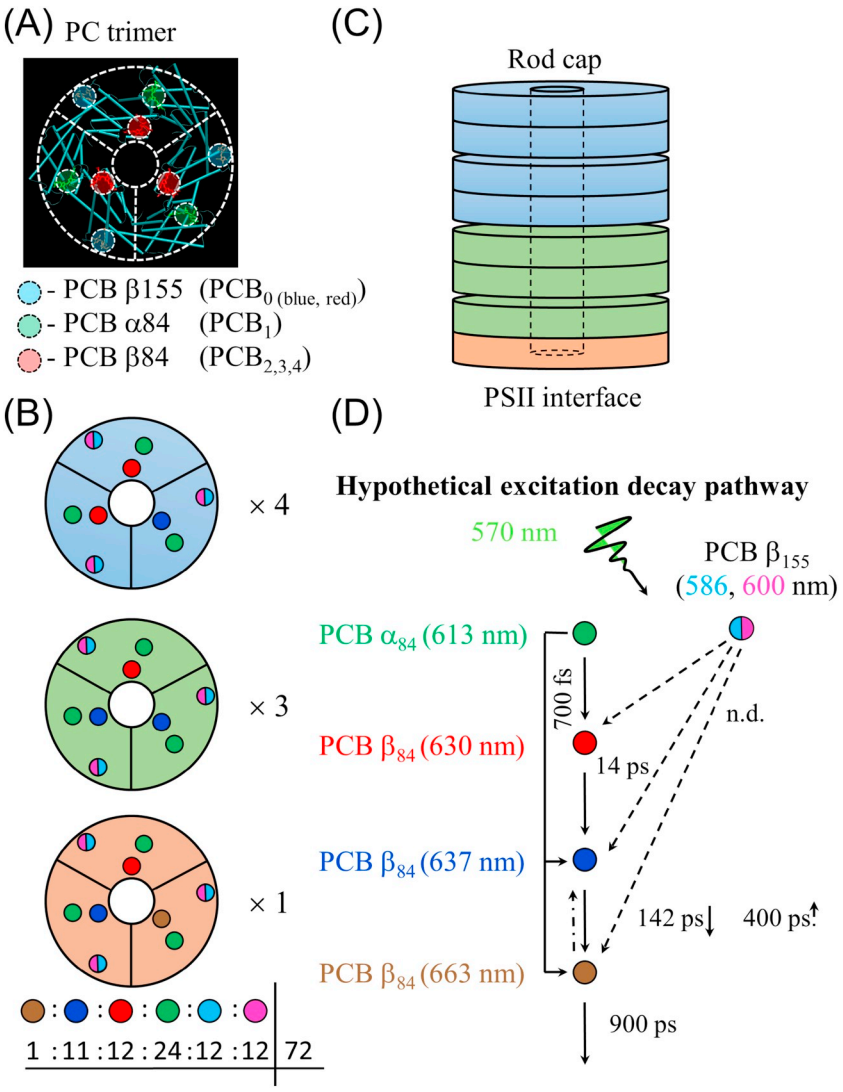

Fig. 9. Schematic spatial distribution of various spectral forms of α and β PCBs in the lWL PBS rod that fits to outcomes from spectroscopic analysis and that will warrant excitation migration toward the end of rod attached to the photosynthetic membrane. (A) The structural model of PC trimer is based on 1HA7 structure from PDB protein databank; (B) hypothetical distribution of PCB spectral forms within PC trimers and (C) color-coded AmPBS assembly; (D) hypothetical excitation decay pathways after excitation at 570 nm. n.d. – not determined.

3.6. Is PC structural heterogeneity behind lWL AmPBS functionality?

A valid question to ask here is how the spectral heterogeneity among set of essentially structurally identical PC trimers is achieved upon assembly to the lWL AmPBS rod so it ensures unidirectional flow of the excitation toward a specific end of the rod? Or, in other words, what is the driving factor behind the red-shift of PCB(β_{84}) in PC trimers closer to the membrane side of the rod? If the lWL AmPBS is completely disassembled to AmPC timers, those are essentially identical in spectroscopic properties.

The recent structure of monomeric AmPC from the same type of AmPBS as studied here demonstrated that the AmPC monomer exists in isoforms and some structural variability in position of cofactors around PCB(α_{84}) and PCB(β_{84}) chromophores is noticeable [16]. It cannot be excluded that spectral heterogeneity of PCB(β_{84}) are indeed due to small structural differences in environments surrounding those pigments. This heterogeneity may be compounded by the presence of either of the two CpcG linker forms (belonging to the rod-core linker family). Both forms were found to be present in AmPBS isolated from lWL at about the same amount. The role of this linker may be different from one in the PBSs from other species, as there is no core. Certainly, this is an interesting issue and demands further investigation in the future.

Transparency document

The Transparency document associated with this article can be found, in online version.

Acknowledgments

This work was supported by the United States-Israel Binational Science Fundation (2014395) and the Israel Science Foundation founded by the Israel Academy of Sciences and Humanities (843/16) and support from the Nancy & Stephen Grand Technion Energy Program (GTEP). DNM and the spectroscopic work was supported by the Photosynthetic Antenna Research Center, an Energy Frontier Research Center funded by the U.S. Department of Energy, Office of Science, Office of Basic Energy Sciences under Award Number DE-SC 0001035.

References

[1] A. Wilde, C.W. Mullineaux, Light-controlled motility in prokaryotes and the problem of directional light perception, FEMS Microbiol. Rev. 41 (2017) 900–922.
[2] L. Li, E.-M. Aro, A.H. Millar, Mechanisms of photodamage and protein turnover in photoinhibition, Trends Plant Sci. 23 (2018) 667–676.
[3] N. Adir, H. Zer, S. Shochat, I. Ohad, Photoinhibition - a historical perspective, Photosynth. Res. 76 (2003) 343–370.
[4] A. Soitamo, V. Havurinne, E. Tyystjärvi, Photoinhibition in marine picocyanobacteria, Physiol. Plant. 161 (2017) 97–108.
[5] N. Murata, S. Takahashi, Y. Nishiyama, S.I. Allakhverdiev, Photoinhibition of photosystem II under environmental stress, Biochim. Biophys. Acta Bioenerg. 1767 (2007) 414–421.
[6] A.R. Grossman, M.R. Schaefer, G.G. Chiang, J.L. Collier, The phycobilisome, a light-harvesting complex responsive to environmental conditions, Microbiol. Rev. 57 (1993) 725–749.
[7] S. Bailey, A. Grossman, Photoprotection in cyanobacteria: regulation of light harvesting, Photochem. Photobiol. 84 (2008) 1410–1420.
[8] F. Gan, D.A. Bryant, Adaptive and acclimative responses of cyanobacteria to far-red light, Environ. Microbiol. 17 (2015) 3450–3465.
[9] D. Kirilovsky, C.A. Kerfeld, Cyanobacterial photoprotection by the orange carotenoid protein, Nat. Plants 2 (2016) 16180.
[10] J. Zhang, J. Ma, D. Liu, S. Qin, S. Sun, J. Zhao, S.-F. Sui, Structure of phycobilisome from the red alga *Griffithsia pacifica*, Nature 551 (2017) 57–63.
[11] H. Miyashita, H. Ikemoto, N. Kurano, K. Adachi, M. Chihara, M. Shigetoh, Chlorophyll d as a major pigment, Nature 383 (1996) 402.
[12] J. Marquardt, H. Senger, H. Miyashita, S. Miyachi, E. Moerschel, Isolation and characterization of biliprotein aggregates from *Acaryochloris marina*, a Prochloron-like prokaryote containing mainly chlorophyll d, FEBS Lett. 410 (1997) 428–432.
[13] Q. Hu, J. Marquardt, I. Iwasaki, H. Miyashita, N. Kurano, E. Morschel, S. Miyachi, E. Mo, S. Miyachi, Molecular structure, localization and function of biliproteins in the chlorophyll a/d containing oxygenic photosynthetic prokaryote *Acaryochloris marina*, Biochim. Biophys. Acta Bioenerg. 1412 (1999) 250–261.
[14] C. Theiss, F.J. Schmitt, J. Pieper, C. Nganou, M. Grehn, M. Vitali, R. Olliges, H.J. Eichler, H.J. Eckert, Excitation energy transfer in intact cells and in the phycobiliprotein antennae of the chlorophyll d containing cyanobacterium *Acaryochloris marina*, J. Plant Physiol. 168 (2011) 1473–1487.
[15] N. Adir, Elucidation of the molecular structures of components of the phycobilisome: reconstructing a giant, Photosynth. Res. 85 (2005) 15–32.
[16] S. Bar-Zvi, A. Lahav, D. Harris, D.M. Niedzwiedzki, R.E. Blankenship, N. Adir, Structural heterogeneity leads to functional homogeneity in *A. marina* phycocyanin, Biochim. Biophys. Acta Bioenerg. 1859 (2018) 544–553.
[17] M. Chen, M. Floetenmeyer, T.S.S. Bibby, Supramolecular organization of phycobiliproteins in the chlorophyll d-containing cyanobacterium *Acaryochloris marina*, FEBS Lett. 583 (2009) 2535–2539.
[18] M. Watanabe, M. Ikeuchi, Phycobilisome: architecture of a light-harvesting supercomplex, Photosynth. Res. 116 (2013) 265–276.
[19] I.N. Stadnichuk, P.M. Krasilnikov, D.V. Zlenko, Cyanobacterial phycobilisomes and phycobiliproteins, Microbiology 84 (2015) 101–111.
[20] R.S. Gloag, R.J. Ritchie, M. Chen, A.W.D. Larkum, R.G. Quinnell, Chromatic photoacclimation, photosynthetic electron transport and oxygen evolution in the Chlorophyll d-containing oxyphotobacterium *Acaryochloris marina*, Biochim. Biophys. Acta Bioenerg. 1767 (2007) 127–135.
[21] H. Schiller, H. Senger, H. Miyashita, S. Miyachi, H. Dau, Light-harvesting in *Acaryochloris marina*-spectroscopic characterization of a chlorophyll d-dominated photosynthetic antenna system, FEBS Lett. 410 (1997) 433–436.
[22] L. David, M. Prado, A.A. Arteni, D.A. Elmlund, R.E. Blankenship, N. Adir, Structural studies show energy transfer within stabilized phycobilisomes independent of the mode of rod-core assembly, Biochim. Biophys. Acta Bioenerg. 1837 (2014) 385–395.
[23] D.M. Niedzwiedzki, J. Jiang, C.S. Lo, R.E. Blankenship, Low-temperature spectroscopic properties of the peridinin-chlorophyll a-protein (PCP) complex from the coral symbiotic dinoflagellate *Symbiodinium*, J. Phys. Chem. B 117 (2013) 11091–11099.
[24] D.M. Niedzwiedzki, T. Tronina, H. Liu, H. Staleva, J. Komenda, R. Sobotka, R.E. Blankenship, T. Polívka, Carotenoid-induced non-photochemical quenching in the cyanobacterial chlorophyll synthase–HliC/D complex, Biochim. Biophys. Acta Bioenerg. 1857 (2016) 1430–1439.
[25] E.R. Henry, J. Hofrichter, Singular value decomposition: application to analysis of experimental data, Methods Enzymol. 210 (1992) 129–192.
[26] I.H.M. van Stokkum, D.S. Larsen, R. van Grondelle, Global and target analysis of time-resolved spectra, Biochim. Biophys. Acta Bioenerg. 1657 (2004) 82–104.
[27] D. Bhaya, In the limelight: photoreceptors in cyanobacteria, MBio 7 (2016).
[28] M. Ikeuchi, T. Ishizuka, Cyanobacteriochromes: a new superfamily of tetrapyrrole-binding photoreceptors in cyanobacteria, Photochem. Photobiol. Sci. 7 (2008) 1159–1167.
[29] Y. Hirose, N.C. Rockwell, K. Nishiyama, R. Narikawa, Y. Ukaji, K. Inomata, J.C. Lagarias, M. Ikeuchi, Green/red cyanobacteriochromes regulate complementary chromatic acclimation via a protochromic photocycle, Proc. Natl. Acad. Sci. U. S. A. 110 (2013) 4974–4979.
[30] H.-B. Mao, G.-F. Li, D.-H. Li, Q.-Y. Wu, Y.-D. Gong, X.-F. Zhang, N.-M. Zhao, Effects of glycerol and high temperatures on structure and function of phycobilisomes in *Synechocystis* sp. PCC 6803, FEBS Lett. 553 (2003) 68–72.
[31] A.C.C. Nganou, L. David, N. Adir, D. Pouhe, M.J.J. Deen, M. Mkandawire, Evidence of additional excitation energy transfer pathways in the phycobiliprotein antenna system of *Acaryochloris marina*, Photochem. Photobiol. Sci. 14 (2015) 429–438.
[32] C. Nganou, Low absorption state of phycocyanin from *Acaryochloris marina* antenna system: on the interplay between ionic strength and excitonic coupling, J. Chem. Phys. 139 (2013) 045101.
[33] D.M. Niedzwiedzki, C.N. Hunter, R.E. Blankenship, Evaluating the nature of so-called S*-state feature in transient absorption of carotenoids in light-harvesting complex 2 (LH2) from purple photosynthetic bacteria, J. Phys. Chem. B 120 (2016) 11123–11131.
[34] J.L. Herek, T. Polívka, T. Pullerits, G.J. Fowler, C.N. Hunter, V. Sundström, Ultrafast carotenoid band shifts probe structure and dynamics in photosynthetic antenna complexes, Biochemistry 37 (1998) 7057–7061.
[35] J.L. Herek, M. Wendling, Z. He, T. Polivka, G. Garcia-Asua, R.J. Cogdell, C.N. Hunter, R. van Grondelle, V. Sundstrom, T. Pullerits, Ultrafast carotenoid band shifts: experiment and theory, J. Phys. Chem. B 108 (2004) 10398–10403.
[36] W. Liptay, Dipole moments and polarizabilities of molecules in excited electronic states, in: E.C. Lim (Ed.), Excited States, Academic Press, New York, 1974, pp. 129–229.
[37] M.P. Debreczeny, K. Sauer, J. Zhou, D.A. Bryant, Monomeric C-phycocyanin at room temperature and 77 K: resolution of the absorption and fluorescence spectra of the individual chromophores and the energy-transfer rate constants, J. Phys. Chem. B 97 (1993) 9852–9862.
[38] I. Eisenberg, F. Caycedo-Soler, D. Harris, S. Yochelis, S.F. Huelga, M.B. Plenio, N. Adir, N. Keren, Y. Paltiel, Regulating the energy flow in a cyanobacterial light-harvesting antenna complex, J. Phys. Chem. B 121 (2017) 1240–1247.
[39] G. Gryliuk, M. Ratsep, S. Hildebrandt, K.D. Irrgang, H.J. Eckert, J. Pieper, Excitation energy transfer and electron-vibrational coupling in phycobiliproteins of the cyanobacterium Acaryochloris marina investigated by site-selective spectroscopy, Biochim. Biophys. Acta Bioenerg. 1837 (2014) 1490–1499.
[40] A.K. Padyana, V.B. Bhat, K.M. Madyastha, K.R. Rajashankar, S. Ramakumar, Crystal structure of a light-harvesting protein C-phycocyanin from Spirulina platensis, Biochem. Biophys. Res. Commun. 282 (2001) 893–898.
[41] M.P. Debreczeny, K. Sauer, J. Zhou, D.A. Bryant, Comparison of calculated and experimentally resolved rate constants for excitation energy transfer in C-phycocyanin. 2. Trimers, J. Phys. Chem. 99 (1995) 8420–8431.
[42] T. Gillbro, A.V. Sharkov, I.V. Kryukov, E.V. Khoroshilov, P.G. Kryukov, R. Fischer, H. Scheer, Förster energy transfer between neighbouring chromophores in C-phycocyanin trimers, Biochim. Biophys. Acta Bioenerg. 1140 (1993) 321–326.
[43] J.M. Womick, A.M. Moran, Nature of excited states and relaxation mechanisms in C-phycocyanin, J. Phys. Chem. B 113 (2009) 15771–15782.
[44] R.E. Riter, M.D. Edington, W.F. Beck, Isolated-chromophore and exciton-state photophysics in C-phycocyanin trimers, J. Phys. Chem. B 101 (1997) 2366–2371.
[45] Y.L. Ren, B. Chi, O. Melhem, K. Wei, L.L. Feng, Y.J. Li, X.Y. Han, D. Li, Y. Zhang, J. Wan, X. Xu, M.H. Yang, Understanding the electronic energy transfer pathways in the trimeric and hexameric aggregation state of cyanobacteria phycocyanin within the framework of forster theory, J. Comput. Chem. 34 (2013) 1005–1012.
[46] A.R. Holzwarth, J. Wendler, G.W. Suter, Studies on chromophore coupling in isolated phycobiliproteins, Biophys. J. 51 (1987) 1–12.
[47] M.P. Debreczeny, K. Sauer, J. Zhou, D.A. Bryant, Comparison of calculated and experimentally resolved rate constants for excitation energy transfer in C-phycocyanin. 1. Monomers, J. Phys. Chem. 99 (1995) 8412–8419.
[48] L.J. Tian, M. Gwizdala, I.H.M. van Stokkum, R.B.M. Koehorst, D. Kirilovsky, H. van Amerongen, Picosecond kinetics of light harvesting and photoprotective quenching in wild-type and mutant phycobilisomes isolated from the cyanobacterium *Synechocystis* PCC 6803, Biophys. J. 102 (2012) 1692–1700.
[49] I.H.M. van Stokkum, M. Gwizdala, L.J. Tian, J.J. Snellenburg, R. van Grondelle, H. van Amerongen, R. Berera, A functional compartmental model of the *Synechocystis* PCC 6803 phycobilisome, Photosynth. Res. 135 (2018) 87–102.